Uroporphyrinogen III Synthase Knock-In Mice Have the Human Congenital Erythropoietic Porphyria Phenotype, Including the Characteristic Light-Induced Cutaneous Lesions

David F. Bishop,[1,*] Annika Johansson,[1,*] Robert Phelps,[2] Amr A. Shady,[1] Maria C. M. Ramirez,[1] Makiko Yasuda,[1] Andres Caro,[3] and Robert J. Desnick[1]

Departments of [1]Human Genetics, [2]Dermatology, and [3]Pharmacology and Biological Chemistry, Mount Sinai School of Medicine, New York

Congenital erythropoietic porphyria (CEP), an autosomal recessive inborn error, results from the deficient but not absent activity of uroporphyrinogen III synthase (URO-synthase), the fourth enzyme in the heme biosynthetic pathway. The major clinical manifestations include severe anemia, erythrodontia, and disfiguring cutaneous involvement due to the accumulation of phototoxic porphyrin I isomers. Murine models of CEP could facilitate studies of disease pathogenesis and the evaluation of therapeutic endeavors. However, URO-synthase null mice were early embryonic lethals. Therefore, knock-in mice were generated with three missense mutations, C73R, V99A, and V99L, which had in vitro–expressed activities of 0.24%, 5.9%, and 14.8% of expressed wild-type activity, respectively. Homozygous mice for all three mutations were fetal lethals, except for mice homozygous for a spontaneous recombinant allele, $V99A^T/V99A^T$, a head-to-tail concatemer of three V99A targeting constructs. Although $V99A^T/V99A^T$ and $C73R/V99A^T$ mice had ~2% hepatic URO-synthase activity and normal hepatic microsomal heme and hemoprotein levels, they had 20% and 13% of wild-type activity in erythrocytes, respectively, which indicates that sufficient erythroid URO-synthase was present for fetal development and survival. Both murine genotypes showed marked porphyrin I isomer accumulation in erythrocytes, bone, tissues, and excreta and had fluorescent erythrodontia, hemolytic anemia with reticulocytosis and extramedullary erythropoiesis, and, notably, the characteristic light-induced cutaneous involvement. These mice provide insight into why CEP is an erythroid porphyria, and they should facilitate studies of the disease pathogenesis and therapeutic endeavors for CEP.

Congenital erythropoietic porphyria (CEP [MIM 263700]), also known as "Günther disease," is an autosomal recessive inborn error of heme biosynthesis due to the low but not absent activity of uroporphyrinogen III synthase (URO-synthase [EC 4.2.1.75]) (Romeo and Levin 1969; Anderson et al. 2001). This enzyme catalyzes the cyclization and isomerization of the linear tetrapyrrole hydroxymethylbilane (HMB; aka "preuroporphyrinogen") to uroporphyrinogen III (Burton et al. 1979; Jordan et al. 1979; Battersby et al. 1980). In the absence of URO-synthase activity, HMB rapidly cyclizes nonenzymatically to the nonphysiologic uroporphyrinogen I isomer (Burton et al. 1979), which is metabolized to coproporphyrinogen I. Uroporphyrinogen I and coproporphyrinogen I are oxidized to their respective porphyrin I isomers: uroporphyrin (URO) I and coproporphyrin (COPRO) I. Thus, the deficient *UROS* activity in CEP results in incomplete metabolism of HMB and an accumulation of the pathologically toxic URO and COPRO I isomers.

The human URO-synthase gene, located on chromosome 10q26.2, has alternative housekeeping and erythroid-specific promoters whose mRNAs both encode the 265-aa, 29-kDa monomeric enzyme (Aizencang et al. 2000*a*, 2000*b*). To date, >35 URO-synthase mutations have been identified in patients with CEP (Human Gene Mutation Database) (Stenson et al. 2003), including 22 missense mutations whose mutant enzymes have varying amounts of residual activity (see, e.g., Desnick and Astrin 2002). In fact, the presence and severity of clinical manifestations in CEP depend on the amount of residual URO-synthase activity and range from nonimmune hydrops fetalis to a milder, later-onset form with only cutaneous photosensitivity and compensated hemolysis (Anderson et al. 2001; Desnick and Astrin 2002). Thus, phenotype-genotype correlations have been established for certain URO-synthase mutations (reviewed by Desnick and Astrin [2002]).

The major manifestations of CEP include hemolytic anemia and cutaneous photosensitivity (Anderson et al. 2001; Desnick and Astrin 2002; Bickers and Frank 2003). Anemia due to erythrocyte hemolysis can be life-threatening if the marrow cannot compensate, and severely affected patients are transfusion dependent.

Received January 3, 2006; accepted for publication January 25, 2006; electronically published February 9, 2006.

Address for correspondence and reprints: Dr. R. J. Desnick, Professor and Chairman, Department of Human Genetics, Box 1498, Mount Sinai School of Medicine, Fifth Avenue at 100th Street, New York, NY 10029. E-mail: rjdesnick@mssm.edu

* These two authors contributed equally to this work.

Am. J. Hum. Genet. 2006;78:645–658. 0002-9297/2006/7804-0011$15.00

Splenomegaly and splenic sequestration may cause pancytopenia (Anderson et al. 2001). Other manifestations include erythrodontia and bone loss (Piomelli et al. 1986; Fritsch et al. 1997; Anderson et al. 2001). Hemolysis releases the toxic porphyrin I isomers into the circulation, with subsequent deposition in the skin, bone, other tissues, feces, and urine. Exposure to sunlight and other UV sources results in cutaneous photosensitivity, manifested by blistering of the epidermis in sun-exposed areas. The subepidermal bullae and vesicles are prone to rupture, and secondary infection leads to cutaneous scarring and deformities, including loss of digits, eyelids, nostrils, and ears. Corneal scarring can lead to blindness. Hypertrichosis of the face and extremities is common (Poh-Fitzpatrick 1986), and extensive pigment changes, including hyperpigmentation and depigmentation, occur in minimally exposed areas. The skin and corneal damage presumably results from the phototoxic excitation of the accumulated URO and COPRO I isomers, producing singlet oxygen with subsequent lipid peroxidation and membrane damage following exposure to sunlight (Kaufman et al. 1967; Dawe et al. 2002; Bickers and Frank 2003). However, the pathogenic mechanism of the dermal photosensitivity has not been investigated, primarily because of the lack of an animal model of CEP.

For severely affected patients, bone marrow transplantation (BMT) has been curative (Shaw et al. 2001; Dupuis-Girod et al. 2005). However, BMT requires at least a haploidentical match and is associated with a significant risk of morbidity and mortality. Thus, efforts have been directed to develop stem-cell gene therapy for CEP (e.g., Kauppinen et al. 1998; Mazurier et al. 2001; Geronimi et al. 2003). Although the success of BMT has provided the rationale for gene-replacement strategies, the major obstacle to preclinical studies of the safety and effectiveness of various therapeutic endeavors is the lack of a CEP animal model.

A previous effort to develop a knockout mouse model of human CEP was unsuccessful because URO-synthase homozygous null mice were embryonic lethals at the 4–8 cell stage (Bensidhoum et al. 1998), and heterozygotes had no CEP phenotype. Therefore, on the basis of human mutant alleles, we selected murine URO-synthase missense mutations that encoded a range of residual activities (from ~0.25% to 15% of in vitro–expressed wild-type activity) to generate murine knock-in (KI) models of CEP. Here, we report the generation of mice heterozygous for the common severe C73R, milder V99A, and synthetic V99L mutations. Mice homozygous for these mutations were fetal lethals, with the exception of a fortuitous recombination event involving triplication of the V99A targeting construct that resulted in homozygous mice with <2% of wild-type activity in liver but ~20% of wild-type activity in erythrocytes. $V99A^T/V99A^T$ and $C73R/V99A^T$ mice had the characteristic CEP biochemical and clinical phenotypes, including systemic porphyrin accumulation, prominent fluorescent erythrodontia, fluorescent peripheral erythrocytes, and hemolytic anemia with reticulocytosis and decreased haptoglobin levels (Bishop et al. 2004, 2005). The $V99A^T/V99A^T$ and $C73R/V99A^T$ genotypes were transferred onto the hairless albino background (SKH1 strain) to facilitate studies of the skin photosensitivity. After loading with 5-aminolevulinic acid (ALA) to accelerate porphyrin accumulation, these mice developed the typical light-induced cutaneous involvement and dermatopathology. These mice provide viable murine models of CEP that should facilitate investigation of disease pathogenesis and therapy.

Material and Methods

Cloning and Expression of Mutant Murine URO-Synthase Alleles

The 798-bp murine wild-type cDNA coding sequence for URO-synthase (GenBank accession number NM_009479) was subcloned into the pKK223-3 vector (Amersham Biosciences) at the *Eco*RI (5′) and *Xma*I (3′) restriction sites and was designated "pKK-WT." Mutant constructs pKK-C73R, pKK-V99A, and pKK-V99L were generated by site-directed mutagenesis by use of the QuickChange method (Stratagene). To avoid introduction of PCR-induced mutations in the vector, each mutant construct was digested with *Bst*XI and *Xho*I, after which the 415-bp cassette carrying the respective mutation was subcloned into the corresponding position in pKK-WT, the sequence was confirmed, and then each was used to transform *Escherichia coli* DH5α competent cells (Invitrogen). After growth in Luria broth cultures, induction, and cell lysis, the supernatant URO-synthase enzymatic activity was measured as described elsewhere (Tsai et al. 1987), except that the erythrocyte lysate used to generate HMB-synthase was replaced by 5 units of homogeneous recombinant human HMB-synthase (purified after expression in *E. coli*; 1 unit of enzyme activity was equal to 1 nmol of HMB produced per h under the conditions of the assay). For assays of URO-synthase in saline-perfused mouse tissues, the HMB-synthase concentration was increased to 10 units per assay. Protein concentrations were measured using the Bradford protein assay (Bio-Rad).

Construction of the Targeting Vectors and Generation of KI Mice

A genomic murine URO-synthase fragment was isolated from mouse strain 129/OLA embryonic stem (ES) cells (Aizencang et al. 2000*b*). The targeting replacement vectors contained a 10.6-kb URO-synthase genomic fragment from intron 1 to intron 6 and had the C73R, V99A, or V99L mutation introduced into exon 4 or 5, with adjacent, silent *Avr*II (for exon 4 mutation) or *Hae*II (for exon 5 mutations) restriction sites. A neomycin-resistance selection cassette (*neo*) was introduced into intron 4 for positive selection with G418 (fig. 1). The primers used for vector construction and genotyping are

provided in table 1. Each targeting vector was sequence confirmed. Homologous recombination was performed in 129/Sv/Ev/Tac ES cells, with all three constructs electroporated simultaneously; >300 *neo*-selected clones were isolated, and DNA was extracted and screened for correctly targeted replacements. One positive ES clone each was isolated for the C73R and V99L mutations, and two positive clones were identified for the V99A mutation. After generation of chimeric mice, PCR-based genotyping of offspring by amplification of exon 4 or 5 and restriction analysis of the *Avr*II site introduced adjacent to the exon 4 mutation or the *Hae*II site introduced adjacent to the exon 5 mutations were used to select founder mice for each mutation (fig. 1). Details of vector construction and the generation and selection of ES clones and transgenic mice are given in table 1 and appendix A. Chimeras were mated with BL/6 mice, and germline mutant mice were mated with wild-type or heterozygous littermates. The URO-synthase mutations were also transferred onto the hairless albino SKH1 background.

Animal Studies

Blood was collected from the retro-orbital plexus in EDTA-coated microhematocrit tubes (StatSpin) from animals under open-drop isoflurane anesthesia, and tissues were harvested after euthanization, were quick-frozen in liquid nitrogen, and were stored at −95°C. Hematologic indices were obtained using a Beckman-Coulter model LH-755 hematology analyzer. Plasma haptoglobin levels were determined by a solid-phase ELISA (Life Diagnostics). Feces and urine were collected in metabolic cages every 24 h from individual mice. URO-synthase enzymatic activity was measured in prokaryotic cell lysates, as described above.

Table 1

Primers Used for KI Vector Construction and Genotyping

The table is available in its entirety in the online edition of *The American Journal of Human Genetics*.

Porphyrin Quantification

Porphyrin isomers in urine, feces, plasma, erythrocytes, liver, and enzyme assays were analyzed by high-performance liquid chromatography of the free-acid isomers, as described elsewhere (Lim and Peters 1986; Lim et al. 1988; Kennedy and

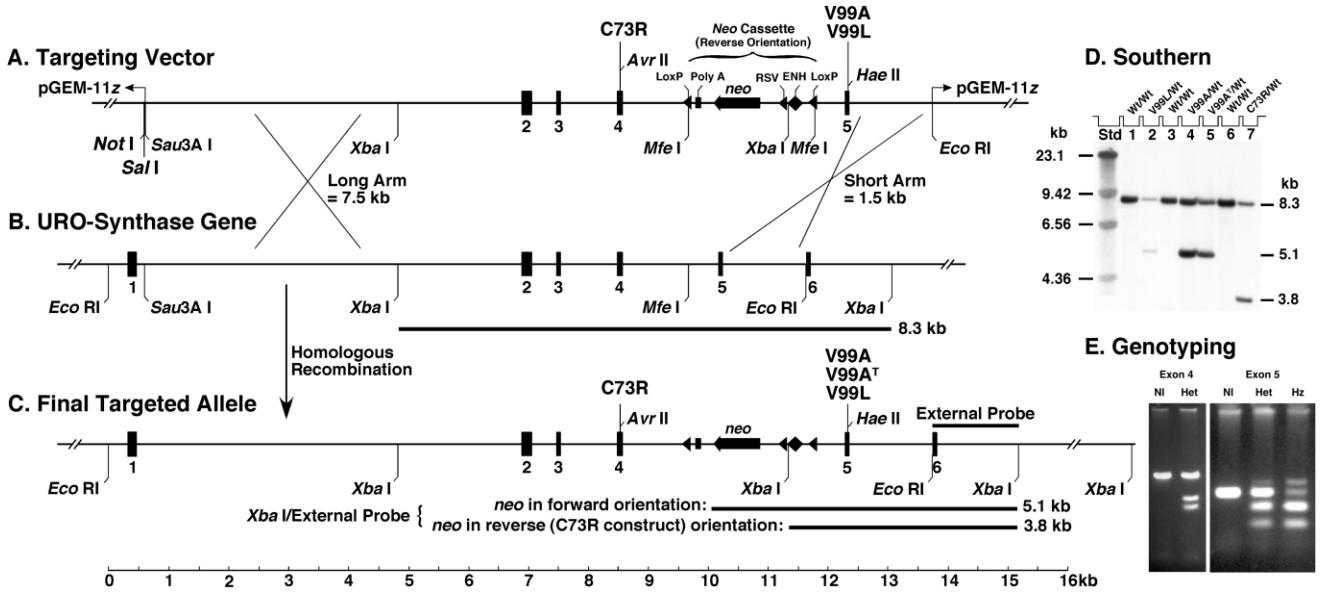

Figure 1 Targeting of hypomorphic mutations into the murine URO-synthase gene by homologous recombination. *A,* Targeting vector. The 11-kb URO-synthase gene sequence of the targeting construct in the pGEM-11Z vector contained a 2-kb floxed *neo*-selectable marker cassette driven by the Rous sarcoma virus (RSV) promoter and four copies of the GTIIC-GTI enhancer cloned into the *Mfe*I site of intron 4. For the exon 4 C73R construct, the *neo* cassette was cloned in the reverse orientation. For the exon 5 V99A and V99L mutations, the *neo* cassette was in the forward orientation. *B,* URO-synthase gene. The wild-type URO-synthase gene restriction map of the potential recombination region is shown. *C,* Final targeted alleles. The targeted alleles showing the inserted mutations and marker gene in the reverse (corresponding to the C73R allele) orientation are shown. The 1.5-kb *Eco*RI/*Xba*I external probe detects the 8.3-kb wild-type and 3.8-kb recombinant *Xba*I restriction fragments for genotype analysis. For the other targeted alleles with the *neo* cassette in the forward orientation, the recombinant *Xba*I fragment is 5.1 kb. *D,* Southern hybridization. Genomic DNA isolated from G418-selected ES cell clones was digested with *Xba*I and was analyzed by Southern hybridization as described in the "Material and Methods" section. The exon 4 and 5 regions of the positive clones were amplified, and the PCR products were sequenced, to confirm the C73R mutation (*lane 7*), the V99L mutation (*lane 2*), and the V99A mutation (*lanes 4 and 5*). The Std lane contains trace-labeled *Hin*dIII λ marker DNA. Wt = wild type. *E,* Genotyping assay. Genomic DNA was amplified with primer pairs U5 and U6 (table 1) and was digested with *Avr*II and *Hae*II for exons 4 and 5, respectively. For exon 4, the wild-type 249-bp band was cut into 112- and 137-bp fragments, and, for exon 5, the 169-bp band was cut into 59- and 110-bp fragments. Het = heterozygote; Hz = homozygote; Nl = normal.

James 1993), by use of a 250 × 4.6–mm BDS Hypersil column (Thermo-Hypersil), with detection by a Waters Model 474 flow fluorometer (excitation wavelength 405 nm; emission wavelength 618 nm; gain 100; attenuation 32). Porphyrins in unfixed blood smears were visualized with an Olympus Model BX61 motorized fluorescence microscope fitted with an oil-immersion 100× UPLANFl objective, a Texas Red fluorescence filter block, an Applied Imaging Model ER-3339 cooled CCD camera, and the Applied Imaging Cytovision version 3.1 image-capture software.

Phenobarbital Treatment and Quantitation of Microsomal Hemoproteins

Approximately 1-mo-old male mice were treated with 120 mg/kg phenobarbital intraperitoneally and were sacrificed with saline perfusion of tissues after 40 h. Livers were harvested from wild-type and knockout mice after overnight starvation, were minced, were homogenized in 0.15 M potassium phosphate buffer (pH 7.4; 5 ml/g liver), and were centrifuged at 12,000 *g* for 15 min. The supernatant was centrifuged at 105,000 *g* for 90 min. Microsomal pellets were washed twice in the resuspension buffer, with centrifugation at 105,000 *g* for 60 min, were resuspended in 50 mM potassium phosphate buffer (pH 7.4; 20 mg protein/ml), were stored at −80°C, and were used within 3 mo (Janzen et al. 1994).

The determination of cytochrome P450 and cytochrome b5 concentrations was done by differential spectrophotometry in accord with the method of Omura and Sato (1964). For cytochrome b5, reduced nicotinamide adenine dinucleotide (NADH) was used as reducing agent, and $\varepsilon_{424-409} = 185\ mM^{-1}\ cm^{-1}$ for the reduced minus oxidized spectrum. For cytochrome P450, sodium dithionite was used as reducing agent, and $\varepsilon_{450-490} = 91\ mM^{-1}\ cm^{-1}$ for the reduced-CO minus reduced spectrum. Protein concentration was determined using the Bio-Rad DC Protein assay. The heme content was measured using the pyridine hemochromogen method (Schenkman and Jansson 1998), with $\varepsilon_{557-575} = 32.4\ mM^{-1}\ cm^{-1}$ for the reduced minus oxidized spectra.

Cutaneous Photosensitivity and Pathology

For the cutaneous photosensitivity studies only, the V99A^T/V99A^T, C73R/V99A^T, and wild-type mice were given 15 mM ALA in their water ad lib for a 10-d period, to accelerate porphyrin accumulation. Starting on day 2 of ALA treatment, the SKH1 wild-type and mutant mice were exposed to four GE F15T8-BLB–Black Light fluorescent bulbs in two UVP Model XX-15 bench lamps at a distance of 20 cm. The bulbs filtered out light above 420 nm, and a Plexiglas filter was added that was selected to block UV light below 400 nm. Thus, most of the light was from the mercury line emission at 405 nm, the Soret absorbance wavelength responsible for porphyrin fluorescence. Exposures were for 12 h per d during the daytime. The mice were sacrificed on day 18, skin was fixed for pathology, and all tissue samples were sectioned, stained with hematoxylin and eosin and/or with periodic acid–Schiff (PAS), mounted, and examined by light microscopy.

The thickness of folded skin in the shaved or hairless area was measured after initiation of light exposure each day at least three times, parallel to and near the backbone, with a Fisherbrand Traceable digital calipers (Fisher Scientific). Dorsal skin from the mice was fixed in neutral buffered formalin overnight and was cut into multiple longitudinal strips and prepared for histopathology in accordance with previously published methods (Phelps et al. 1993).

Results

Generation of URO-Synthase KI Mice

Prokaryotic expression of the murine C73R and V99A alleles resulted in 0.24% and 5.9%, respectively, of expressed wild-type activities, similar to the activities of the corresponding human mutations (<1% and 5.6%), whereas the expressed V99L mutation had 14.8% of wild-type activity (table 2). Targeting vectors (see fig. 1) for each of the three hypomorphic alleles were mixed together and were electroporated into ES cells. Recombinant clones for the three targeted alleles and a fourth variant, a triplicated V99A targeted allele (designated V99A^T), were obtained from the single electroporation procedure. Heterozygous founder mice were generated for all three correctly targeted mutations plus the V99A^T variant. Segregation analysis revealed that all homozygous mice were fetal lethals, except for the variant V99A^T line (table 3). Southern analyses of genomic DNAs with the 3′-flanking probe revealed the expected fragments for all targeted lines, and sequence analysis of both targeted exons 4 and 5 in each case confirmed the presence of both the mutations and adjacent silent restriction sites (fig. 1 and appendix A). However, Southern hybridization of the V99A^T line with the *neo* probe and sequencing of RT-PCR products from cellular RNA (data not shown) revealed a head-to-tail concatemer of three V99A targeting constructs that had inserted between exons 1 and 6 of the URO-synthase gene, as shown schematically in figure 2. Remarkably, sequence analysis showed that the third and most 3′ copy of exon

Table 2

Prokaryotic Expression of Murine and Human URO-Synthase Missense Mutations

	Human[a]		Murine[b]	
Genotype	Activity (U/mg protein)	%WT[c]	Activity (U/mg protein)	%WT[c]
Wild type	77.6	100	864 ± 50	100
C73R	<.8	<1.0	2.1 ± 1.2	.24
V99A	4.3	5.6	51 ± 16	5.9
V99L	NA[d]	NA[d]	128 ± 54	14.8

[a] Human enzymatic activity in (expressed in prokaryotes) reported by Xu et al. (1995) and Warner et al. (1992).

[b] Mean (±SD) activity measured in bacterial lysates; see the "Material and Methods" section for details.

[c] Percentage of wild-type activity levels.

[d] NA = not applicable. V99L has not been reported in human patients with CEP.

Table 3

Segregation of KI Mutations

Mating	F1 Offspring					χ^2	P	Conclusion
	No. of Litters	Total Offspring	No. of +/+ Mice	No. of +/− Mice	No. of −/− Mice			
WT/C73R × WT/C73R	20	148	64	84	0	58.1	$<10^{-8}$	C73R/C73R = lethal
WT/V99A × WT/V99A	20	159	54	105	0	53.0	$<10^{-8}$	V99A/V99A = lethal
WT/V99A^T × WT/V99A^T	3	27	4	15	8	1.52	.468	V99A^T/V99A^T = viable
WT/V99L × WT/V99L	20	168	53	115	0	56.3	$<10^{-8}$	V99A/V99A = lethal

Note.—Chimeras generated from implantation of the selected ES cell clones were mated with wild-type (WT) BL/6, CD1, or SV129 mice, and the litters were genotyped as described in the "Material and Methods" section. For χ^2 analysis, the Chi-Square calculator (see Web Resources) was used.

5 in the V99A^T recombinant contained the inserted *Hae*II restriction site but not the more 5′ V99A mutation present in the other two copies (fig. 2). RT-PCR studies indicated barely detectable levels of the housekeeping transcript, which is needed for viability, presumably the result of splicing exon 1 to the last copy of exon 2B in the concatemer (fig. 2). The other abundant transcripts containing exon 1 were alternatively spliced with triplicated exons 2–5, which would encode truncated enzyme polypeptides. In contrast, RT-PCR of the erythroid-specific transcript revealed a single wild-type fragment length, indicating transcription by the erythroid promoter of the most 3′ copy in the V99A^T concatemer, which had reverted to wild type (V99). Semiquantitative RT-PCR of total RNA from perfused spleens indicated that expression of the housekeeping and erythroid transcripts in the V99A^T/V99A^T mice was ~3% and ~30%, respectively, of expression in spleens from wild-type mice. These levels were similar to the housekeeping enzyme activity in liver and the combined housekeeping and erythroid activities in spleen (table 4). Of note, the V99A^T allele expressed wild-type and not mutant housekeeping or erythroid enzyme activities.

URO-Synthase Activities and Porphyrin Levels in the V99A^T/V99A^T and C73R/V99A^T Mice

The hepatic, splenic, and erythrocytic URO-synthase activities in the V99A^T/V99A^T, C73R/V99A^T, and wild-type BL/6 mice are shown in table 4. The hepatic activities in the V99A^T/V99A^T and C73R/V99A^T mice were 2.1% and 1.5% of wild-type, respectively, whereas the erythrocytic activities were 20% and 13% of wild-type and splenic activities were 44% and 32% of wild-type, respectively. These findings were compatible with the RT-PCR results that showed very low levels of housekeeping transcripts but moderately abundant erythroid transcripts. Splenic activities were markedly increased in these mice and presumably reflect erythroid URO-synthase activity from extramedullary erythropoiesis. When these genotypes were transferred to the hairless albino SKH1 background, hepatic, erythrocytic, and splenic URO-synthase activities similar to those on the BL/6 background were observed (table 4).

Compared to wild-type concentrations, the total I isomer (URO I plus COPRO I) concentrations in the V99A^T/V99A^T and C73R/V99A^T BL/6 mice were, respectively, 2- and 25-fold greater in erythrocytes, 5- and 6-fold greater in plasma, 39- and 31-fold greater in urine, and 62- and 108-fold greater in feces, with the majority of fecal type I isomer being COPRO I (83% and 94%, respectively), which is more soluble in bile (table 5). Of note, URO I in the perfused livers of C73R/V99A^T BL/6 mice was elevated 60-fold from wild-type levels, indicating a hepatic component of porphyrin I accumulation. In contrast, the levels of the porphyrin III isomers were maximally increased only 4- and 6-fold above wild-type levels for V99A^T/V99A^T and C73R/V99A^T BL/6 mice, respectively (table 5), which indicates that the deficient URO-synthase activities stimulated biosynthesis of HMB, presumably because of the increased activity of ALA-synthase, the rate-determining step of the pathway (Anderson et al. 2001). When the V99A^T/ V99A^T and C73R/V99A^T genotypes were transferred to the SKH1 background, similar I isomer increases were observed in erythrocytes and plasma, whereas the increase was more marked in urine and less marked in feces (table 5). The life spans of the CEP mice were not different from the wild-type life span of ~2 years.

Bone, Tooth, and Erythroid Cell Fluorescence

V99A^T/V99A^T and heteroallelic C73R/V99A^T, V99A/V99A^T, and V99L/V99A^T mice were viable and had marked porphyrin accumulation in bones, including fluorescent erythrodontia (fig. 3*A*–3*D*), which is pathognomonic for CEP and served as a diagnostic marker for homozygous and heteroallelic mice. UV illumination of newborn mice with a Wood's lamp (Gupta and Singhi 2004) displayed the fluorescent porphyrin-laden skeleton (fig. 3*A* and 3*B*). The fluorescence intensity of the bones and teeth was inversely correlated with the residual URO-synthase activity; the C73R/V99A^T mice had

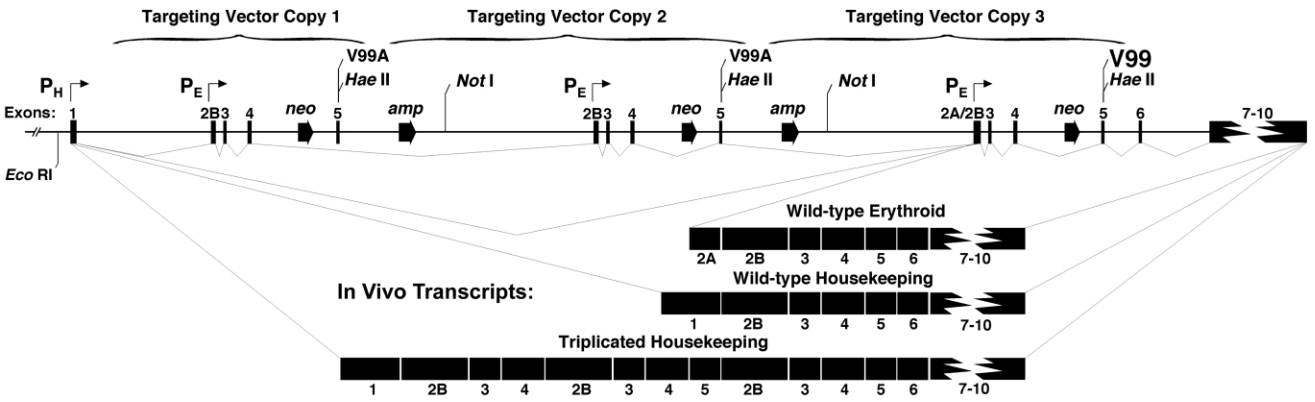

Figure 2 Diagram of the V99A^T triplicated recombinant allele and major transcripts. Southern and sequence analyses of the PCR products from reverse-transcribed and amplified liver mRNA from the homozygous V99A^T mice revealed alternatively spliced transcripts and the presence of at least three copies of exons 2B–5 inserted between exons 1 and 6 of the transgene. Other transcripts were identified with exon 5 present or skipped in the first and/or second repeats. The *Not*I site was used for linearization of the vector. P_H and P_E indicate the transcription start sites directed by the housekeeping and erythroid promoters, respectively. The ampicillin-resistance gene (*amp*) was retained in two copies of the concatemerized insert.

brighter bones and teeth than those of V99A^T homozygotes (not shown). Fluorescence microscopy of peripheral erythrocytes from these mice revealed occasional highly fluorescent cells (fig. 3*F*), as is seen in human patients with CEP.

Hematology

The hematologic indices for 16–18-mo-old wild-type/wild-type, V99A^T/V99A^T, and C73R/V99A^T BL/6 mice were similar for erythrocyte counts, hematocrits, hemoglobin concentrations, mean corpuscular hemoglobin, mean corpuscular volume, and total leukocyte counts (table 6). However, the reticulocyte counts in the C73R/V99A^T mice were markedly increased (33% vs. 8% in wild-type mice), and erythrocyte hemolysis was evidenced by the 10-fold decrease in plasma haptoglobin (1.2 ng/ml vs. 10.4 ng/ml in wild-type mice) (table 6). The increased hemolysis, presumably caused by the increased erythrocyte porphyrin I isomers, stimulated erythropoiesis, as evidenced by the reticulocytosis and higher splenic URO-synthase activity (table 4), which is consistent with a compensated hemolytic anemia. Splenomegaly in the C73R/V99A^T mice was variable, with splenic weights ranging from normal to five times normal (based on percentage of total body weight). Although the marrow appeared morphologically normal in wild-type and C73R/V99A^T mice, variably increased erythropoiesis and increased iron deposits were evident in C73R/V99A^T spleens.

Heme Content of Hepatic Microsomal Hemoproteins

To determine whether the 98% reduction of URO-synthase activity in the liver compromised hemoprotein biosynthesis, phenobarbital, which induces both heme synthesis and cytochrome P450, was administered to wild-type and C73R/V99A^T BL/6 mice to place an additional demand on heme synthesis. In wild-type mice, the P450 content was reduced 75% at 40 h after phenobarbital administration, whereas the reduction in C73R/V99A^T mice was only 43% (fig. 4). For cytochrome b5, the reduction was more modest: 36% and 15% for wild-type and CEP mice, respectively (fig. 4). Cytochromes P450 and b5 accounted for ~45% of the total microsomal heme in both wild-type and mutant mice. Interestingly, the sum of the two microsomal cytochromes and the total microsomal heme were 50% higher in C73R/V99A^T mice than in wild-type mice, indicating that, contrary to heme synthesis being compromised, it was elevated in the CEP mice. The reduction in microsomal heme after phenobarbital administration has been reported previously in rats and is presumably a result of secondary induction of heme oxygenase by increased heme levels (Correia and Burk 1978; Sun et al. 2002).

Cutaneous Photosensitivity

To assess the effect of 405-nm light on the skin of wild-type, V99A^T/V99A^T, and C73R/V99A^T mice, the mutant genotypes were transferred onto the hairless albino SKH1 background, and 15 mM ALA was added to the drinking water to accelerate porphyrin I isomer accumulation, as described in the "Material and Methods" section. The plasma porphyrin I isomer concentrations immediately increased in all treated mice to 2–3-fold higher than those in untreated mice, with an overall increase of I isomer concentrations in the mutant mice of 8–10-fold above wild-type levels (table 5). After ex-

Table 4

URO-Synthase Activities in KI Mice

Mice and Genotype	Liver		Erythrocytes		Spleen	
	Activity (U/mg protein)	%WT[a]	Activity (U/mg protein)	%WT[a]	Activity (U/mg protein)	%WT[a]
BL/6:						
WT/WT	8.72 ± 1.23	100	20.1 ± .2	100	7.40 ± 2.40	100
$V99A^T/V99A^T$	.18 ± .05	2.1	4.04 ± .56	20	3.25 ± 1.14	44
$C73R/V99A^T$	.13 ± .02	1.5	2.69 ± .10	13	2.36 ± .34	32
SKH1:						
WT/WT	10.3 ± 1.7	100	15.0 ± 4.9	100	14.9 ± 4.7	100
$V99A^T/V99A^T$	.40 ± .10	3.9	4.6 ± 1.3	34	7.4 ± 1.3	50
$C73R/V99A^T$	.22 ± .14	2.1	1.4 ± .2	9.3	1.8 ± .5	12

Note.—Data are mean (±SD) for three adult mice (aged 2–4 mo, except for SKH1 spleens, which are from mice aged 2–8 mo).

[a] Percentage of wild-type (WT) activity levels.

posure to 405-nm light for 10 d, bifold skin thickness in the $C73R/V99A^T$ mice increased twofold (from a mean of 0.6 mm to a mean of 1.3 mm; $n = 3$), whereas there was no skin thickening in the wild-type or $V99A^T/V99A^T$ mice. Histopathologic examination of the wild-type skin showed no evidence of acute or chronic photodamage, showing a normal-thickness epidermis (10 μm), and the dermis (367 μm) was free of any significant infiltrate or fibrosis (fig. *5A*). Typical of hairless albino mice, numerous small cysts (remnants of aborted hair follicles) were present in the deeper dermis. Similarly, the $V99A^T/V99A^T$ mice showed slight thickening of the epidermis (30 μm) (fig. *5B* and inset), whereas the dermis (290 μm) was not thickened, consistent with a very mild porphyrin photosensitivity. In marked contrast, the $C73R/V99A^T$ mice showed evidence of the characteristic light-induced cutaneous pathology of human CEP (fig. *5C–5F*). As shown in fig. *5C,* both the epidermis and adnexa showed considerable acanthosis (51 μm) with a focally compact horn, whereas the thickened dermis (480 μm) had a minimal mononuclear infiltrate extending almost to the panniculus carnosus (fig. *5C*). Figure *5D* shows the classic cutaneous pathology of CEP: a noninflammatory, subepidermal bulla with clear-cut separation of the neutrophil-coated full-thickness epidermal roof from the dermal floor, containing rare flattened basal keratinocytes, which most likely represent reepithelization from adjacent rudimentary follicles (fig. *5D*). Compared to unaffected skin from wild-type mice (fig. *5E*), ectatic capillaries were observed in the superficial dermis of a $C73R/V99A^T$ mouse beneath the bullae, and there was a thickening of the walls when stained with PAS (fig. *5F*).

Discussion

Studies of the pathophysiology of CEP and efforts to evaluate therapeutic endeavors have been hindered by the lack of an animal model. Previous efforts to generate a knockout mouse model of CEP by gene targeting were unsuccessful because URO-synthase activity is required for embryonic viability (Bensidhoum et al. 1998). Similarly, homozygous knockout mice for other heme biosynthetic enzymes have also been fetal lethals (Lindberg et al. 1996; Phillips et al. 2001), emphasizing the essential role of heme for embryonic development. Here, we report the successful generation of murine models of human CEP. Although our original strategy was based on introducing missense mutations with residual URO-synthase activities varying from ~0.25% to 15% of the prokaryotically expressed murine wild-type activity (table 2), none of the correctly targeted homozygous mice were viable. Fortuitously, an aberrant triplicated V99A targeting vector produced viable homozygous $V99A^T/V99A^T$ BL/6 mice that had URO-synthase activities of ~2% and ~20% of wild-type in liver and erythrocytes, respectively (table 4). When bred with the C73R heterozygotes, the $C73R/V99A^T$ heteroallelic BL/6 mice were more severely affected, having ~50% lower hepatic and erythrocytic URO-synthase activities (consistent with the essentially null activity of the C73R allele), higher levels of porphyrin accumulation (tables 4 and 5), lower haptoglobin levels, higher reticulocyte counts, more prominent erythrodontia, and variable splenomegaly.

It is notable that the $V99A^T/V99A^T$ and $C73R/V99A^T$ mice were viable with <2% of wild-type hepatic activity but had as low as ~13% of wild-type erythroid activity. Assays of total hepatic microsomal heme and the major hepatic hemoproteins showed that microsomal heme and cytochromes P450 and b5 were maintained at essentially normal or elevated levels relative to wild-type when the mice were treated with phenobarbital (fig. 4). These findings suggest that low levels of hepatic URO-synthase are compatible with the production of the major hepatic hemoproteins, even though there was a 60-fold increase in porphyrin I isomers in the liver. That

Table 5

Porphyrin Isomer Levels in URO-Synthase BL/6 and SKH1 KI Mice

Mice, Tissue, and Genotype	URO I	Total I Isomers[a]	Fold Increase over WT[b]	URO III	Total III Isomers[a]	Fold Increase over WT[b]
BL/6:						
Erythrocytes (nmol/liter):						
WT/WT	1.2 ± .2	4.2 ± .6	1	11 ± 1	13 ± 1	1.0
$V99A^T/V99A^T$	4.2 ± .8	8.0 ± .8	2	13 ± 1	14 ± 1	1.1
$C73R/V99A^T$	64.9 ± 36.2	103 ± 56	25	19 ± 5	22 ± 5	1.7
Plasma (nmol/liter):						
WT/WT	8.8 ± 1.6	9.6 ± 1.6	1.0	.58 ± .36	6 ± 2	1.0
$V99A^T/V99A^T$	25 ± 4	47 ± 15	4.9	3.24 ± .20	17 ± 5	2.8
$C73R/V99A^T$	30 ± 10	61 ± 17	6.4	2.08 ± .55	14 ± 3	2.3
Post-ALA plasma (nmol/liter):						
WT/WT	8.7 ± 5.1	12 ± 4	1.2[c]	7.4 ± 9.6	17 ± 14	2.8[c]
$V99A^T/V99A^T$	67 ± 24	91 ± 27	1.9[c]	18 ± 8.6	33 ± 29	1.9[c]
$C73R/V99A^T$	91 ± 30	123 ± 42	2.0[c]	21 ± 14	22 ± 9	1.6[c]
Urine (nmol/24 h):						
WT/WT	.12 ± .01	.14 ± .01	1.0	.06 ± .00	.14 ± .05	1.0
$V99A^T/V99A^T$	3.3 ± .6	5.4 ± .7	39	.12 ± .02	.38 ± .06	2.8
$C73R/V99A^T$	2.3 ± .9	4.4 ± 1.1	31	.09 ± .04	.54 ± .13	4.0
Feces (nmol/24 h):						
WT/WT	.32 ± .06	.74 ± .15	1.0	.15 ± .02	1.2 ± .3	1.0
$V99A^T/V99A^T$	7.7 ± 4.6	46 ± 18	62	.56 ± .25	4.6 ± 1.5	3.8
$C73R/V99A^T$	4.9 ± 1.0	80 ± 25	108	.53 ± .10	7.3 ± 1.8	6.1
Liver (nmol/24 h):						
WT/WT	2.05 ± .73	2.05 ± .73	1.0	1.14 ± .33	1.14 ± .33	1.0
$C73R/V99A^T$	123 ± 53	125 ± 54	61	2.75 ± .09	2.75 ± .09	2.4
SKH1:						
Erythrocytes (nmol/liter):						
WT/WT	3.3 ± 4.0	3.9 ± 4.2	1.0	.94 ± .55	1.7 ± 1.2	1.0
$V99A^T/V99A^T$	29 ± 14	33 ± 12	8.5	5.0 ± .8	8.1 ± 2.4	4.8
$C73R/V99A^T$	73 ± 36	91 ± 45	23	6.2 ± 1.3	11 ± 1.0	6.5
Plasma (nmol/liter):						
WT/WT	2.9 ± 1.1	5.1 ± 1.3	1.0	1.3 ± .7	3.5 ± 1.5	1.0
$V99A^T/V99A^T$	12 ± 5	31 ± 7	6.1	2.1 ± .7	5.7 ± 2.5	1.6
$C73R/V99A^T$	17 ± 2	43 ± 6	8.4	2.2 ± .6	5.4 ± .8	1.5
Post-ALA plasma (nmol/liter):						
WT/WT	7.0 ± 6.3	9.2 ± 7.3	1.8[c]	5.2 ± 5.1	12 ± 11	3.4[c]
$V99A^T/V99A^T$	66 ± 84	94 ± 124	3.0[c]	28 ± 46	46 ± 67	8.1[c]
$C73R/V99A^T$	46 ± 35	76 ± 40	1.8[c]	32 ± 26	46 ± 29	8.5[c]
Urine (nmol/24 h):						
WT/WT	.02 ± .01	.04 ± .02	1.0	.02 ± .01	.16 ± .04	1.0
$V99A^T/V99A^T$	1.9 ± 1.6	5.0 ± 4.1	120	.08 ± .07	.82 ± 1.05	5.1
$C73R/V99A^T$	4.9 ± 3.0	8.6 ± 3.2	210	.28 ± .11	.53 ± .16	3.3
Feces (nmol/24 h):						
WT/WT	2.2 ± 1.1	3.8 ± 2.2	1.0	.36 ± .27	2.9 ± 1.8	1.0
$V99A^T/V99A^T$	44 ± 27	94 ± 60	25	3.4 ± 2.2	8.7 ± 4.6	3.0
$C73R/V99A^T$	18 ± 3	124 ± 12	33	.52 ± .12	7.5 ± 2.4	2.6

[a] Total I isomers = URO I + COPRO I; total III isomers = URO III + COPRO III. Values are the average of levels in three mice aged 1–2 mo.

[b] Fold increase over the wild-type total isomers, except for post-ALA plasma, for which the isomer values are the average daily amounts over the entire supplementation period and the fold increase is from mice before ALA loading.

[c] The variation in the porphyrin levels in post-ALA plasma is presumably a result of the varying consumption of water containing 15 mM ALA.

such low hepatic URO-synthase activity does not cause the encephalopathy manifested by the acute porphyrias may be explained by the fact that the normal activity of murine URO-synthase is ~50-fold greater than that of HMB-synthase (Bishop and Desnick 1982), the enzymatic defect in acute intermittent porphyria. Thus, 2% of wild-type activity in the liver appears to be sufficient to produce adequate levels of heme for the hepatic hemoproteins. In contrast, the levels of erythroid URO-synthase activity in the KI mice (up to 13% of normal in

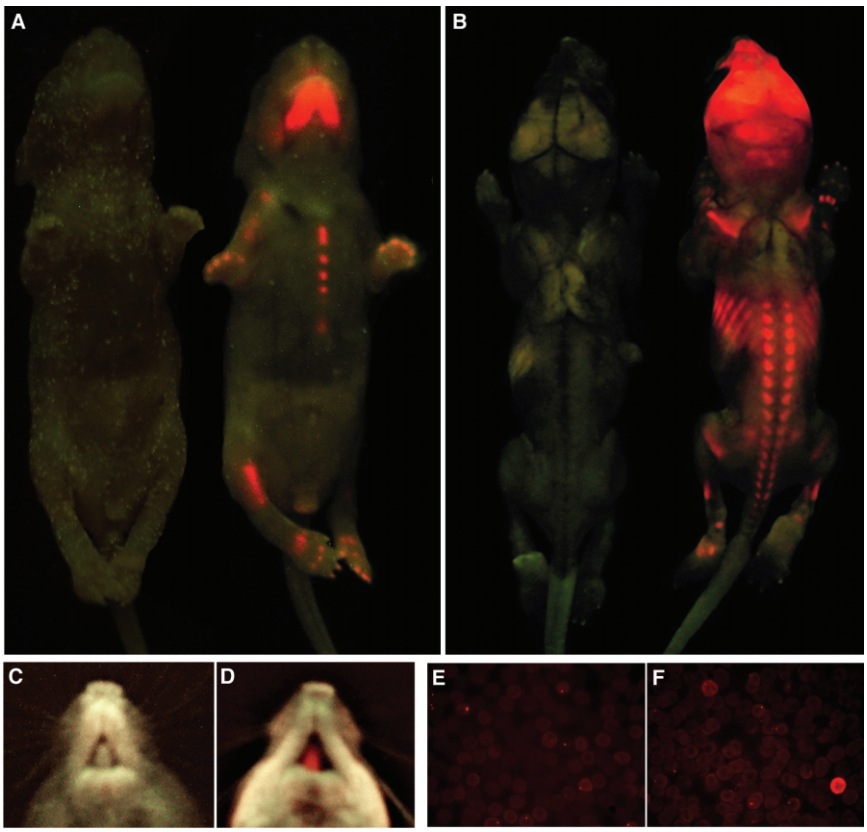

Figure 3 Tooth, bone, and erythrocyte cell fluorescence in C73R/V99A^T mice. Newborn C73R/V99A^T mice had easily visualized erythrodontia, seen using a Wood's lamp, and their bones displayed marked porphyrin fluorescence. Illumination was as described in the "Material and Methods" section for cutaneous exposure, and images were captured at f 2.8 for 1 s and ISO 100 on a 3.2-megapixel digital camera with a Wratten #4 filter. *A,* Euthanized C57BL/6 mice, aged 1–2 d, ventral view, with wild-type mouse at left and C73R/V99A^T mouse at right. *B,* Same mice as in panel A (wild-type at left, C73R/V99A^T at right) but dorsal view after skin removal. *C,* Wild-type mouse at age 31 d. *D,* C73R/V99A^T mouse at age 41 d. *E,* Peripheral blood smear of a wild-type mouse, final magnification × ~500. *F,* Peripheral blood smear of a C73R/V99A^T mouse, final magnification × ~500.

erythrocytes; up to 32% of normal in spleen) (table 4) were not sufficient to prevent biochemical or clinical pathology. The mice had a compensated hemolytic anemia, as evidenced by their 10-fold reduced plasma haptoglobin levels and by their ~4-fold elevated reticulocyte counts, and increased splenic URO-synthase activity, consistent with extramedullary hematopoiesis. These findings indicate that sufficient erythroid URO-synthase activity is critical for normal hematopoiesis and, most importantly, for murine fetal development, since the correctly targeted V99A homozygotes, which have 6% of wild-type activity, were fetal lethals even after removal of the *neo* cassette. Taken together, these findings provide the first pathophysiologic explanation of why URO-synthase deficiency does not result in a hepatic porphyria with acute neurologic attacks but rather in an erythropoietic porphyria with cutaneous manifestations. Moreover, these mice provide a human disease model to investigate the effects of BMT on the erythroid and hepatic contributions to disease pathogenesis, particularly because hepatic and erythroid porphyrin production may increase after puberty (Guarini et al. 1994).

Phenotypically, the clinical severity in human CEP has been shown to correlate with the amount of residual URO-synthase activity encoded by the patient's URO-synthase mutations (Anderson et al. 2001; Desnick and Astrin 2002). The most common and severest human genotype that is variably viable, C73R/C73R, presents as nonimmune hydrops fetalis, or, if surviving to delivery, the newborn has a transfusion-dependent anemia and marked cutaneous photosensitivity. Moderately severe genotypes may have a milder transfusion-dependent or compensated hemolytic anemia and experience severe cutaneous photosensitivity, whereas milder genotypes may have only cutaneous photosensitivity. When exposed to light, all patients develop the characteristic skin lesions, which may be mild to severe, depending on the level of residual URO-synthase activity and light ex-

posure. These lesions can become infected and lead to scarring and disfigurement due to skin and/or bone loss.

The phenotype of the V99A^T/V99A^T and C73R/V99A^T BL/6 or SKH1 mice most closely resembles that of the moderately severe human phenotype. The mice had marked URO I and COPRO I accumulation in erythrocytes, plasma, urine, and feces (table 5); the pathognomonic fluorescent erythrodontia (fig. 3); a fluorescent skeleton; a compensated hemolysis; and the characteristic light-induced cutaneous manifestations. Of note, the porphyrin III isomer levels were greater in the CEP mice than in wild-type mice. This paradoxical finding in the mice also occurs in human CEP and other porphyrias. These CEP mice should allow investigation into the underlying mechanism(s) responsible for this poorly understood phenomenon.

Notably, histologic evaluation of the cutaneous lesions in murine CEP showed that they closely mimicked those in human CEP (Kaufman et al. 1967; Bhutani et al. 1974; Horiguchi et al. 1989), including the characteristic (1) subepidermal bullae; (2) reduplication of the basement membrane around dermal capillaries, as demonstrated by PAS-positive staining; and (3) variable dermal sclerosis. The subepidermal bullae of C73R/V99A^T mice were composed of the characteristic full-thickness epidermis, with dermal papillae forming the floor of the blister. As seen in human CEP, there was no epidermal necrosis or inflammatory infiltrate in the bulla cavity and only a few inflammatory cells in the dermis (fig. 5*C* and 5*D*). The typical reduplication of the basement membrane with thickened PAS-positive material was seen in the prominent capillaries of the dermis—presumably because of the repeated episodes of vascular injury and repeated bullae formation (fig. 5*E* and 5*F*). The characteristic dermal sclerosis of human CEP resulting from continued light-induced injury was also evident in the CEP mice (fig. 5*C* and 5*D*), from the superficial dermis to the panniculus carnosus. Of interest, because hypertrichosis is a known late feature of CEP, there also was massive adnexal hyperplasia (fig. 5*C*). Consistent with the blocking of UVA and UVB radiation, the CEP mice did not show the dermatopathology of UV damage (no areas of confluent necrosis or individually apoptotic keratinocytes). Thus, the ability to generate these lesions by ALA supplementation and controlled illumination should facilitate studies of the pathogenic mechanisms underlying the formation of these lesions, as well as provide a mouse model for studies of their prevention and treatment.

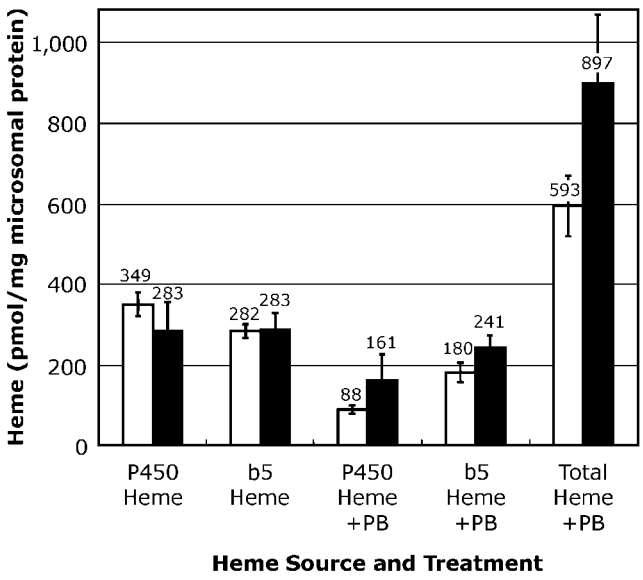

Figure 4 Effect of phenobarbital (PB) on microsomal heme. Isolation and quantitation of total microsomal heme and of microsomal cytochromes P450 and b5 are described in the "Material and Methods" section. The unblackened bars represent wild-type mice, and the blackened bars represent C73R/V99A^T mice. Mean values (*above bars*) are for three mice, and the error bars show ±1 SD.

Recently, Ged et al. (2006) reported a viable homozygous KI mouse model of CEP with the URO-synthase P248Q mutation that had <1% of wild-type erythrocytic activity. Their mice were also generated with SV/129 ES cells, retained the *neo* cassette, and were bred onto the BL/6 background. When expressed in vitro, the human

Table 6

Compensated Hemolytic Anemia in CEP Mice

Genotype	RBC (10^6 cells/ml)	HCT (%)	Hb (g/dl)	MCH (pg)	MCV (fl)	RDW (%)	WBC (10^3 cells/ml)	Reticulocytes[a] (%)	Haptoglobin (ng/ml)
WT/WT	8.7 ± 1.0	41 ± 5	15 ± 2	17 ± 1	47 ± 1	17 ± 2	5.4 ± 2.5	7.9 ± 6.5	10.4 ± 5.7
V99A^T/V99A^T	7.6 ± 1.0	36 ± 4	13 ± 1	17 ± 1	48 ± 2	18 ± 2	4.8 ± 3.7	19 ± 20	8.8 ± 5.1
C73R/V99A^T	8.5 ± 1.4	37 ± 6	14 ± 2	16 ± 1	43 ± 1	21 ± 3	3.0 ± 1.6	33 ± 11	1.2 ± .2

NOTE.—The mean age of the mice was 16 ± 3 mo, and the results are the mean (±SD) of five male mice, except for the haptoglobin data, for which the mean age was 18 ± 2 mo and the results are the mean (±SD) of 4–6 mixed-sex mice. Hb = hemoglobin; HCT = hematocrit; MCH = mean corpuscular hemoglobin; MCV = mean corpuscular volume; RBC = red blood cells; RDW = red cell distribution width; WBC = white blood cells.

[a] For the two-tailed nonparametric Mann-Whitney Wilcoxon test based on the ranks, the mean percentage reticulocyte values for the wild-type and C73R/V99A^T mice were significantly different, with $P < .01$.

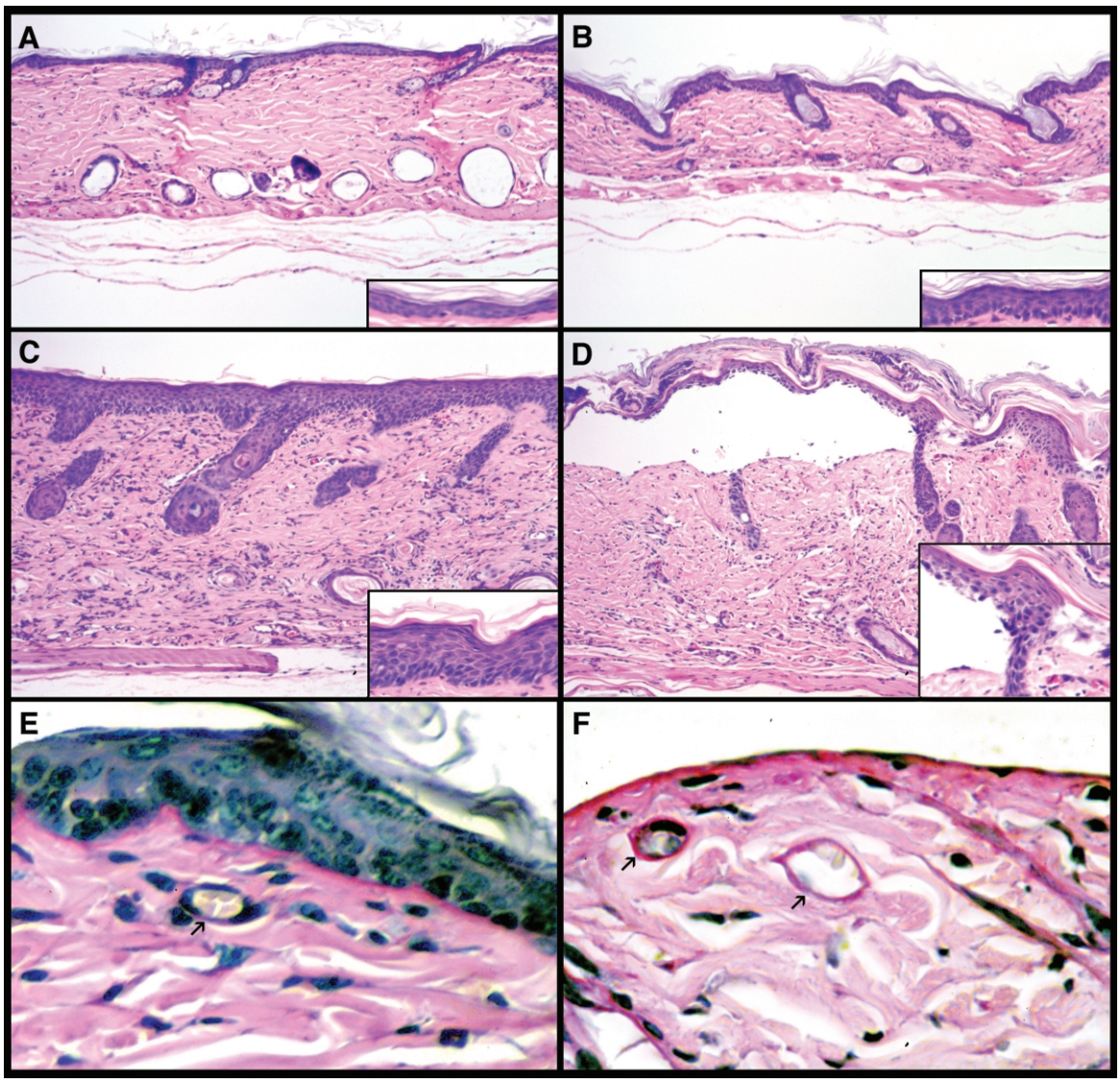

Figure 5 Sections from exposed skin on the backs of SKH1 mice. Panels A–D were stained with hematoxylin and eosin, and panels E and F with PAS. *A* and *E*, Wild-type mouse. *B*, $V99A^T/V99A^T$ mouse. *C*, *D*, and *F*, $C73R/V99A^T$ mice. *A–D*, Magnification ×10, with ×20 insets. *E* and *F*, Magnification ×40.

P248Q allele had ~0.5% of wild-type activity (Fontanellas et al. 1996), which was significantly less than the in vitro activities of the murine V99A or V99L alleles (table 2). Why the homozygous P248Q mice survived while the homozygous V99A and V99L mice with the *neo* cassettes were lethal is not clear. It is notable that when the *neo* cassette was floxed out, the V99L homozygotes were viable, whereas the C73R and V99A homozygotes were not, suggesting an enzymatic survival-threshold effect, similar to that seen in human CEP. Studies are underway to determine at what stage of embryogenesis does lethality occur in the homozygous C73R and V99A mice.

In summary, a viable mouse model of human CEP has been generated by gene targeting with murine missense mutations that encode low levels of URO-synthase activity. The $V99A^T/V99A^T$ and the more severely affected $C73R/V99A^T$ BL/6 and SKH1 mice had biochemical and clinical phenotypes that closely resemble those of patients with moderately severe CEP. These models will enable detailed studies of the underlying mechanisms of the hemolytic anemia and light-induced cutaneous manifestations, particularly the proposed free-radical/singlet-oxygen damage hypothesis (Bickers and Frank 2003). In addition, these mice provide the models required for evaluation of the safety and efficacy of various ther-

apeutic endeavors for CEP, including light-blocking agents, BMT, lentiviral-mediated gene therapy, and novel stem-cell approaches.

Acknowledgments

We thank Drs. Douglas Forrest and Thomas Lufkin, for advice and cassettes for targeting-vector construction; Dr. Paul Frenette, Dr. James Strauchen, and Ms. Mayra Lema, for assistance with microscopy and hematology; Dr. Arthur Cederbaum, for consultation on the hepatic hemoprotein analyses; and Erin O'Hare, Dimitry Gorlik, and Gregory Young, for technical assistance. This research was supported in part by National Institutes of Health grant 5 R01 DK026824. M.R. and Y.M. are recipients of predoctoral and postdoctoral fellowships, respectively, supported by a grant (5 T32 HD07105) from the National Institutes of Health.

Appendix A

Targeting-Vector Construction

The strategy for targeted homologous recombination in ES cells is shown in figure 1. A 14-kb genomic clone containing the entire murine URO-synthase gene was isolated from a 129SV/OLA mouse genomic library (*Sau*3AI partials) in the λ-FIX II vector (Stratagene [catalog number 946305]) as described elsewhere (Aizencang et al. 2000*b*). For generation of the targeting sequence for KI vector construction, an 11-kb *Sal*I/*Eco*RI restriction fragment from this clone extending from 144 bases 3′ of URO-synthase exon 1 to 25 bases 5′ of exon 6 was subcloned into the pGEM11Z vector (Promega) and was designated "pGU1." The entire 11-kb sequence was obtained by automated fluorescent Sanger enzymatic sequencing and from data in the Celera Genomics database. For this and all following constructs, all ligation junctions and synthetic regions were sequence confirmed. For introduction of the three different missense mutations in exons 4 and 5, a 4.5-kb *Bsp*EI-to-*Eco*RI fragment was subcloned from pGU1 into the Litmus-38 vector (New England Biolabs) and was designated "pLU1." Site-directed mutagenesis (QuickChange protocol [Stratagene]) was used to introduce the selected point mutations, along with an additional mutation in a nearby codon wobble position that did not alter the amino acid sequence but created a restriction site for use in ES clone screening. Table 1 lists the mutagenesis primers and the respective mutations introduced in the two exons. For the C73R mutation and adjacent *Avr*II site in exon 4, an internal sequence-confirmed 600-bp *Nsi*I/*Bmg*BI fragment with the desired base changes was removed and ligated into the *Nsi*I/*Bmg*BI–digested original pLU1 construct to generate clone pLU2. For the two exon 5 mutations, V99A and V99L, and their adjacent silent *Hae*II sites, an internal 1,200-bp *Msc*I/*Nhe*I fragment was removed and ligated into the pLU1 construct to yield clones pLU3 and pLU4, respectively. The pLU2, pLU3, and pLU4 clones were each cut with *Bsp*EI and *Eco*RI and were ligated back into *Bsp*EI/*Eco*RI–digested clone pGU1 to generate constructs pGUC73R, pGUV99A, and pGUV99L, respectively.

To introduce a removable *neo*-selection marker into the unique *Mfe*I site in URO-synthase intron 4, an adapter was synthesized using the N1 primer pair (table 1) and was subcloned into *Nsi*I/*Sac*I–digested pGEM9Zf^{+} (Promega) to yield clone pG1. A *neo* insert and flanking LoxP sites from clone pFN1 (kindly provided by Dr. Douglas Forrest, Mount Sinai) were removed with *Spe*I and ligated into the adapter *Spe*I site of clone pG1 to yield clone pGFN1. The *Eco*RI/*Sal*I fragment of pGFN1, internal to the LoxP sequences, was replaced with the *Eco*RI/*Sal*I fragment of a *neo* construct containing a weakened promoter (kindly provided by Dr. Thomas Lufkin, Mount Sinai) to generate clone pGFN2. The *Mfe*I insert of pGFN2 containing the floxed *neo* cistron was then subcloned into the unique *Mfe*I site in intron 4 of plasmids pGUC73R, pGUV99A, and pGUV99L, to generate constructs pGUC73R^{neo}, pGUV99A^{neo}, and pGUV99L^{neo}, respectively. Plasmid pGUC73R^{neo} contained the *neo Mfe*I cassette in the reverse orientation, whereas, in the other constructs, the cassette was in the forward orientation.

Homologous Recombination in ES Cells and Generation of Germline Chimeras

ES cell line TC1 (derived from strain SV129/SvEvTac [Deng et al. 1995; Leder et al. 1997]) was electroporated using a mixture of all three KI constructs linearized with *Not*I, each at a concentration of 1 μg/ml. Three-hundred ES cell clones were selected in G418. Genomic DNA was isolated from ~300 G418-resistant clones, and 10-μg aliquots were digested with *Xba*I and then genotyped by Southern hybridization to a ^{32}P-radiolabeled (by Rediprime II DNA Labeling System [Amersham Pharmacia Biotech]), 1.2-kb external probe between the *Eco*RI and *Xba*I sites immediately flanking exon 6. The external probe was obtained from SV129 DNA by PCR using primer pair U7 (table 1). Positive clones were sequence confirmed for the presence of the specific mutations by amplification and sequencing of exon 4 or 5 (by use of oligonucleotide primer pairs U5 and U6 in table 1) and then were microinjected into C57BL/6 blastocysts and implanted into C57BL/6 pseudo-pregnant foster mothers. The exon 4 KI chimeric males were bred with C57BL/6 females to generate F1 mice, whereas the

F1 generation from the exon 5 KI chimeric males were from out-bred CD1 females. Subsequent generations have been maintained on this mixed C57BL/6–CD1 background.

Genotyping of KI Mouse DNA

Genomic DNA was isolated from toe clips or tail snips as described elsewhere (Laird et al. 1991), with minor modifications. The tissue was diced with a scalpel and was digested overnight with Proteinase K at 55°C in an Eppendorf Model 5436 Thermomixer shaker (at 1,300 rpm [Brinkmann]). After centrifugation for 15 min at 10,000 *g*, the supernatant was mixed with an equal volume of isopropanol by inversion, and the precipitate was isolated as described (Laird et al. 1991) and was washed once in 70% ethanol, followed by rehydration for 1.5 h at 65°C with shaking at 1,300 rpm in the Thermomixer. The exon 4 (249 bp) and exon 5 (169 bp) amplicons generated with primer pairs U4 and U5 (table 4) were digested with *Avr*II and *Hae*II, respectively. Only the mutated amplicons were cleaved; the heterozygous exon 4 amplicon yielded the expected 112- and 137-bp *Avr*II fragments, and the heterozygous exon 5 amplicon yielded the predicted 59- and 110-bp *Hae*II fragments (data not shown). The fragments were visualized by electrophoresis in 3% MetaPhor agarose gels (Cambrex Bio Science).

Web Resources

The accession number and URLs for data presented herein are as follows:

Chi-Square calculator, http://www.unc.edu/~preacher/chisq/chisq.htm
GenBank, http://www.ncbi.nlm.nih.gov/Genbank/ (for URO-synthase cDNA [accession number NM_009479])
Online Mendelian Inheritance in Man (OMIM), http://www.ncbi.nlm.nih.gov/Omim/ (for CEP)

References

Aizencang G, Solis C, Bishop DF, Warner C, Desnick RJ (2000*a*) Human uroporphyrinogen-III synthase: genomic organization, alternative promoters, and erythroid-specific expression. Genomics 70: 223–231

Aizencang GI, Bishop DF, Forrest D, Astrin KH, Desnick RJ (2000*b*) Uroporphyrinogen III synthase: an alternative promoter controls erythroid-specific expression in the murine gene. J Biol Chem 275: 2295–2304

Anderson KE, Sassa S, Bishop DF, Desnick RJ (2001) Disorders of heme biosynthesis: X-linked sideroblastic anemia and the porphyrias. In: Scriver CR, Beaudet AL, Sly WS, Valle D (eds) The metabolic and molecular bases of inherited disease. Vol 2. McGraw-Hill, New York, pp 2991–3062

Battersby AR, Fookes CJR, Matcham GWJ, McDonald E (1980) Biosynthesis of the pigments of life: formation of the macrocycle. Nature 285:17–21

Bensidhoum M, Larou M, Lemeur M, Dierich A, Costet P, Raymond S, Daniel JY, de Verneuil H, Ged C (1998) The disruption of mouse uroporphyrinogen III synthase (uros) gene is fully lethal. Transgenics 2:275–280

Bhutani LK, Sood SK, Das PK, Mulay DN, Kandhari KC, Deshpande SG (1974) Congenital erythropoietic porphyria: an autopsy report. Arch Dermatol 110:427–431

Bickers DR, Frank J (2003) The porphyrias. In: Freedberg I, Eisen A, Wolff K, Austen K, Goldsmith L, Katz S (eds) Fitzpatrick's dermatology in general medicine. Vol 2. McGraw-Hill, New York, pp 1435–1466

Bishop DF, Desnick RJ (1982) Assays of the heme biosynthetic enzymes. Enzyme 28:91–93

Bishop DF, Johansson A, Desnick RJ (2005) Congenital erythropoietic porphyria: generation and characterization of knock-in mouse models [abstract]. J Inher Metab Dis Suppl 1 28:258

Bishop DF, Ramirez MC, Shady A, Desnick RJ (2004) Viable knock-in mouse model of congential erythropoietic porphyria [abstract]. Am J Hum Genet Suppl 74:339

Burton G, Fagerness PE, Hosozawa S, Jordan PM, Scott AI (1979) ^{13}C N.M.R. evidence for a new intermediate, pre-uroporphyrinogen, in the enzymic transformation of porphobilinogen into uroporphyhrinogens I and III. J Chem Soc Chem Commun 5:202–204

Correia MA, Burk RF (1978) Rapid stimulation of hepatic microsomal heme oxygenase in selenium-deficient rats: an effect of phenobarbital. J Biol Chem 253:6203–6210

Dawe SA, Peters TJ, Du Vivier A, Creamer JD (2002) Congenital erythropoietic porphyria: dilemmas in present day management. Clin Exp Dermatol 27:680–683

Deng C, Zhang P, Harper JW, Elledge SJ, Leder P (1995) Mice lacking p21CIP1/WAF1 undergo normal development, but are defective in G1 checkpoint control. Cell 82:675–684

Desnick RJ, Astrin KH (2002) Congenital erythropoietic porphyria: advances in pathogenesis and treatment. Br J Haematol 117:779–795

Dupuis-Girod S, Akkari V, Ged C, Galambrun C, Kebaili K, Deybach JC, Claudy A, Geburher L, Philippe N, de Verneuil H, Bertrand Y (2005) Successful match-unrelated donor bone marrow transplantation for congenital erythropoietic porphyria (Günther disease). Eur J Pediatr 164:104–107

Fontanellas A, Bensidhoum M, Enriquez de Salamanca R, Moruno Tirado A, de Verneuil H, Ged C (1996) A systematic analysis of the mutations of the uroporphyrinogen III synthase gene in congenital erythropoietic porphyria. Eur J Hum Genet 4:274–282

Fritsch C, Bolsen K, Ruzicka T, Goerz G (1997) Congenital erythropoietic porphyria. J Am Acad Dermatol 36:594–610

Ged C, Mendez M, Robert E, Lalanne M, Lamrissi-Garcia I, Costet P, Daniel JY, Dubus P, Mazurier F, Moreau-Gaudry F, de Verneuil H (2006) A knock-in mouse model of congenital erythropoietic porphyria. Genomics 87:84–92

Geronimi F, Richard E, Lamrissi-Garcia I, Lalanne M, Ged C, Redonnet-Vernhet I, Moreau-Gaudry F, de Verneuil H (2003) Lentivirus-mediated gene transfer of uroporphyrinogen III synthase fully corrects the porphyric phenotype in human cells. J Mol Med 81: 310–320

Guarini L, Piomelli S, Poh-Fitzpatrick MB (1994) Hydroxyurea in congenital erythropoietic porphyria [letter]. N Engl J Med 330: 1091–1092

Gupta LK, Singhi MK (2004) Wood's lamp. Indian J Dermatol Venereol Leprol 70:131–135

Horiguchi Y, Horio T, Yamamoto M, Tanaka T, Seki Y, Imamura S (1989) Late onset erythropoietic porphyria. Br J Dermatol 121:255–262

Janzen EG, Poyer JL, West MS, Crossley C, McCay PB (1994) Study of reproducibility of spin trapping results in the use of C-phenyl-N-tert-butyl nitrone (PBN) for trichloromethyl radical detection in CCl4 metabolism by rat liver microsomal dispersions: biological spin trapping I. J Biochem Biophys Methods 29:189–205

Jordan PM, Burton G, Nordlöv H, Schneider MM, Pryde L, Scott AI (1979) Pre-uroporphryinogen: a substrate for uroporphyrinogen III cosynthetase. J Chem Soc Chem Commun 5:204–205

Kaufman BM, Vickers HR, Rayne J, Ryan TJ (1967) Congenital erythropoietic porphyria: report of a case. Br J Dermatol 79:210–220

Kauppinen R, Glass IA, Aizencang G, Astrin KH, Atweh GF, Desnick RJ (1998) Congenital erythropoietic porphyria: prolonged high-level expression and correction of the heme biosynthetic defect by retroviral-mediated gene transfer into porphyric and erythroid cells. Mol Genet Metab 65:10–17

Kennedy SW, James CA (1993) Improved method to extract and concentrate porphyrins from liver tissue for analysis by high-performance liquid chromatography. J Chromatogr 619:127–132

Laird PW, Zijderveld A, Linders K, Rudnicki MA, Jaenisch R, Berns A (1991) Simplified mammalian DNA isolation procedure. Nucleic Acids Res 19:4293

Leder A, Daugherty C, Whitney B, Leder P (1997) Mouse ζ- and α-globin genes: embryonic survival, α-thalassemia, and genetic background effects. Blood 90:1275–1282

Lim CK, Li FM, Peters TJ (1988) High-performance liquid chromatography of porphyrins. J Chromatogr 429:123–153

Lim CK, Peters TJ (1986) High-performance liquid chromatography of uroporphyrin and coproporphyrin isomers. Methods Enzymol 123:383–389

Lindberg RL, Porcher C, Grandchamp B, Ledermann B, Burki K, Brandner S, Aguzzi A, Meyer UA (1996) Porphobilinogen deaminase deficiency in mice causes a neuropathy resembling that of human hepatic porphyria. Nat Genet 12:195–199

Mazurier F, Geronimi F, Lamrissi-Garcia I, Morel C, Richard E, Ged C, Fontanellas A, Moreau-Gaudry F, Morey M, de Verneuil H (2001) Correction of deficient $CD34^+$ cells from peripheral blood after mobilization in a patient with congenital erythropoietic porphyria. Mol Ther 3:411–417

Omura T, Sato R (1964) The carbon monoxide-binding pigment of liver microsomes. I. Evidence for its hemoprotein nature. J Biol Chem 239:2370–2378

Phelps RG, Daian C, Shibata S, Fleischmajer R, Bona CA (1993) Induction of skin fibrosis and autoantibodies by infusion of immunocompetent cells from tight skin mice into C57BL/6 Pa/Pa mice. J Autoimmun 6:701–718

Phillips JD, Jackson LK, Bunting M, Franklin MR, Thomas KR, Levy JE, Andrews NC, Kushner JP (2001) A mouse model of familial porphyria cutanea tarda. Proc Natl Acad Sci USA 98:259–264

Piomelli S, Poh-Fitzpatrick MB, Seaman C, Skolnick LM, Berdon WE (1986) Complete suppression of the symptoms of congenital erythropoietic porphyria by long-term treatment with high-level transfusions. N Engl J Med 314:1029–1031

Poh-Fitzpatrick MB (1986) The erythropoietic porphyrias. Dermatol Clin 4:291–296

Romeo G, Levin EY (1969) Uroporphyrinogen III cosynthase in human congenital erythropoietic porphyria. Proc Natl Acad Sci USA 63: 856–863

Schenkman JB, Jansson I (1998) Spectral analyses of cytochromes P450. Methods Mol Biol 107:25–33

Shaw PH, Mancini AJ, McConnell JP, Brown D, Kletzel M (2001) Treatment of congenital erythropoietic porphyria in children by allogeneic stem cell transplantation: a case report and review of the literature. Bone Marrow Transplant 27:101–105

Stenson PD, Ball EV, Mort M, Phillips AD, Shiel JA, Thomas NS, Abeysinghe S, Krawczak M, Cooper DN (2003) Human Gene Mutation Database (HGMD): 2003 update. Hum Mutat 21:577–581

Sun J, Hoshino H, Takaku K, Nakajima O, Muto A, Suzuki H, Tashiro S, Takahashi S, Shibahara S, Alam J, Taketo MM, Yamamoto M, Igarashi K (2002) Hemoprotein Bach1 regulates enhancer availability of heme oxygenase-1 gene. EMBO J 21:5216–5224

Tsai SF, Bishop DF, Desnick RJ (1987) Coupled-enzyme and direct assays for uroporphyrinogen III synthase activity in human erythrocytes and cultured lymphoblasts: enzymatic diagnosis of heterozygotes and homozygotes with congenital erythropoietic porphyria. Anal Biochem 166:120–133

Warner CA, Yoo HW, Roberts AG, Desnick RJ (1992) Congenital erythropoietic porphyria: identification and expression of exonic mutations in the uroporphyrinogen III synthase gene. J Clin Invest 89:693–700

Xu W, Warner CA, Desnick RJ (1995) Congenital erythropoietic porphyria: identification and expression of 10 mutations in the uroporphyrinogen III synthase gene. J Clin Invest 95:905–912